Structural Engineering and Mechanics, *Vol. 70, No. 4 (2019) 431-443*
DOI: https://doi.org/10.12989/sem.2019.70.4.431

Numerical studies of the failure modes of ring-stiffened cylinders under hydrostatic pressure

Teguh Muttaqie[1,2a], Do Quang Thang[3b], Aditya Rio Prabowo[4c], Sang-Rai Cho[5,6d] and Jung Min Sohn*[1]

[1]Department of Naval Architecture and Marine Systems Engineering, Pukyong National University, Busan, Republic of Korea
[2]Agency for the Assessment and Application of Technology, Center of Technology for Defense and Security Industries - BPPT, Jakarta, Indonesia
[3]Department of Naval Architecture and Ocean Engineering, Nha Trang University, Nha Trang, Viet Nam
[4]Department of Mechanical Engineering, Sebelas Maret University, Surakarta, Indonesia
[5]School of Naval Architecture and Ocean Engineering, University of Ulsan, Republic of Korea.
[6]Ulsan Lab, Inc, Ulsan, Republic of Korea

(Received October 17, 2018, Revised March 6, 2019, Accepted March 8, 2019)

Abstract. The present paper illustrates a numerical investigation on the failure behaviour of ring-stiffened cylinder subjected to external hydrostatic pressure. The published test data of steel welded ring-stiffened cylinder are surveyed and collected. Eight test models are chosen for the verification of the modelling and FE analyses procedures. The imperfection as the consequences of the fabrication processes, such as initial geometric deformation and residual stresses due to welding and cold forming, which reduced the ultimate strength, are simulated. The results show that the collapse pressure and failure mode predicted by the nonlinear FE analyses agree acceptably with the experimental results. In addition, the failure mode parameter obtained from the characteristic pressure such as interframe buckling pressure known as local buckling pressure, overall buckling pressure, and yield pressure are also examined through the collected data and shows a good correlation. A parametric study is then conducted to confirm the failure progression as the basic parameters such as the shell radius, thickness, overall length of the compartment, and stiffener spacing are varied.

Keywords: Ring-stiffened cylinders; collapse pressure; failure mode criterion; hydrostatic pressure test; non-linear FEA

1. Introduction

The submarine pressure hull part is substantial in sustaining the internal pressure from the deep-sea environment while also providing buoyancy to prevent sinking to extreme depths. It is reported in the literatures that the problem of shell instability has been a topic of interest as early as 1858 when Fairbairn (1858) performed the collapse test of the tubes. And Tokugawa (1929) revealed the overall failure mode of stiffening shell for the first time.

In accordance to the earlier numerous theoretical reports in the literature, different well known failure modes have been evaluated for the ring-stiffened cylinder (von Mises 1929; Winderburg and Trilling 1934; Bryant 1954). Fig. 1 shows the different failure possibilities on the submarine, where the ring-stiffened cylinder form is its primary structural member. However, only three primary failures existed purely by the nature of the external hydrostatic pressure.

One of them is shell yielding, where the plate yields like an accordion between the frames (Lunchick 1956; Lunchick and Overby 1961) and the pressure at this point is called yield pressure. Next is the local buckling of the plate between the frames. Both of these failures are due to the plates that are held in between the frames being loaded beyond their capacity. Local buckling often occurs on both sides of the frames. It will be formed as several lobes at the shells known as local failure (Slankard and Nash 1953; Kirstein and Slankard 1956; Miller and Kinra 1981; Frieze 1994; Araar and Julien 1996; Ross *et al.* 2000). The pressure estimation on this characteristic is local buckling pressure. Another case of failure is when the frame and the shell fail together as a unit, known as overall buckling (Ross 1997). These failures occur when the shell is relatively thin compared to the lobe that propagates the frame, and is detrimental to its stiffeners. The critical pressure at this characteristic is overall buckling pressure. In some cases, the local and overall failure modes can interact with each other, known as failure mode interaction (Morandi *et al.* 1996; Graham 2007; Cho *et al.* 2018a).

The most widespread concept of the selection of the dimension of the primary scantling of the stiffener and shell design criteria of is proposed by Kendrick 1982, which is widely received in pressure vessel design codes (BSI 2003). Another separate design criterion is provided to avoid the sideway tripping of the ring stiffeners, in which it has to ensure that the elastic buckling pressure for tripping is at least three times the allowable pressure. Hence, some conservatism exists because of the failure mode being considered separately. In addition, the failure modes

*Corresponding author, Professor
E-mail: jminz@pknu.ac.kr

ISSN: 1225-4568 (Print), 1598-6217 (Online)

Table 1 Properties of the benchmark test model

Base model*	Shell parameters (mm)*			Ring-stiffener parameters (mm)*			Material parameters (GPa)*		References
	L_c	R	t	h_w	t_w	L_s	σ_y	E	
1	691.4	341.6	5.6	31.1	8.4	65.3	0.328	206.0	BR 7, (Lunchick and Overby 1961)
2	950.0	274.5	2.4	25.0	3.9	100.0	0.288	218.8	RS 4, (Cho *et al.* 2018)
3	1060.0	400.0	4.0	35.0	3.9	200.0	0.307	206.0	RS I, (Cho *et al.* 2018)
4	1128.8	337.0	3.4	24.1	5.9	180.6	0.349	206.0	BR 4, (Kirstein and Slankard 1956)
5	1470.0	490.0	7.5	38.0	8.2	163.0	0.588	216.0	W 3, (Yamamoto *et al*, 1989;
6	1920.0	497.5	5.0	24.0	5.0	100.0	0.588	216.0	W 1, (Yokota *et al*. 1985)
7	4915.2	199.0	11.1	78.9	11.2	1550.0	0.261	197.0	No.5, (Miller and Kinra 1981)
8	4915.2	201.0	6.7	37.1	7.0	1239.0	0.270	200.0	No. 18, (Miller and Kinra 1981)

*) The notations are graphically described in Fig. 2 except σ_Y and E (Yield strength and Young's modulus)

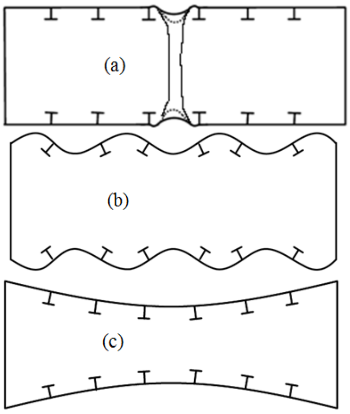

Fig. 1 Possible failure at the center of submarine pressure hull

prediction on the existing design codes are not clear accounted. The improved collapse and failure modes predictions of this conventional design code could be achieved unless the nonlinear finite element analysis (FEA) is incorporated in the design procedure (MacKay *et al.* 2011; 2013).

The extent of this paper is to elaborate the benchmark nonlinear finite element analyses using the characteristic pressure formulae as the basis for the design of a ring-stiffened cylinder. The representative test method collected among the published test reports is presented. Those test results are substantiated using the shell finite element software, ABAQUS FEA. The case of a ring-stiffened cylinder is systematically investigated, starting from the residual stresses due to shell cold bending and stiffener welding. In the sequel, geometrically nonlinear analyses that target the determination of the most appropriate types of imperfections and their characteristics are considered.

The paper is organised as follows. In Section 2, describes the ring-stiffened cylinder models that is typically used in the ultimate strength tests are presented. Section 3 outlines the failure modes of the ring-stiffened cylinder, the formulation of the characteristic pressure. Section 4 presents the detail of nonlinear finite element analysis (FEA) and benchmarking strategies using the chosen legacy test models. The discussion of the complete examination of the characteristic pressure from the numerical results is presented in section 5. Finally, conclusions are summarised in section 6.

2. Details of the ring-stiffened cylinders test models

For over 50 years, the ring-stiffened cylinder ultimate strength has received significant attention from the US and UK Navy. Their investigations were leading to the new understanding of the failure mode for general instability, known as overall buckling (Yokota *et al*. 1985; Morihana *et al*. 1990; Yamamoto *et al*. 1989), and failure mode interaction (Cho *et al*. 2018b). Those test models have the same structural configuration of a pressure hull: a cylindrical shell with T-section ring-stiffeners. Another similar form was also found on offshore structures where those tests have been performed.

The shells are cold-rolled to the required shell radius and subsequently the ring stiffeners are welded to the cylindrical shell. Therefore, the initial shape of imperfection and the residual stress due to forming and welding are induced in the test model to mimic the submarine pressure hull. Among the available test models, only eight test models were chosen for further benchmark analyses and the verification of failure modes. Those are the steel welded flat-bar stiffened cylinder. The geometries and material properties of the ring-stiffened cylindrical models are shown in Table 1.

3. Failure mode under the hydrostatic pressure

When the cylinder failed subjected to the external hydrostatic pressure, the designer prefers the interframe or local buckling to occur instead of overall buckling. This condition will result in a stocky form in the design of the ring stiffener. In the severe case, the local buckling will extend over the entire length of the cylinder when the stiffeners are insufficient, or when the cylinder is long. The failure is the so–called overall buckling. The photographs of the failure modes are summarised in Table 2. As shown in model no.1, the failure mode is shell yielding. Shell yielding may be possible owing the sturdiness of the

Table 2 Failure mode of the benchmark test models

Base model	1	2	3	4
	Shell yield	Local	Interactive	Local
Failure Modes	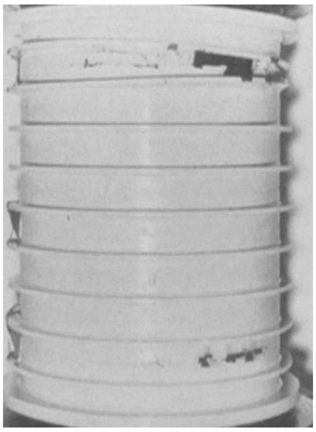			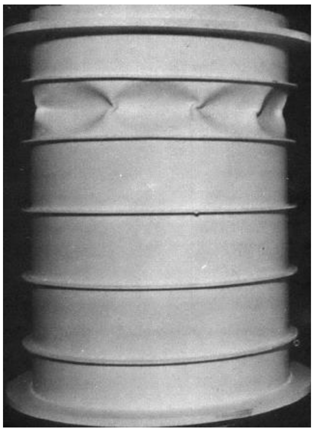
Base model	5	6	7	8
	Overall	Overall	Local	Overall
Failure Modes	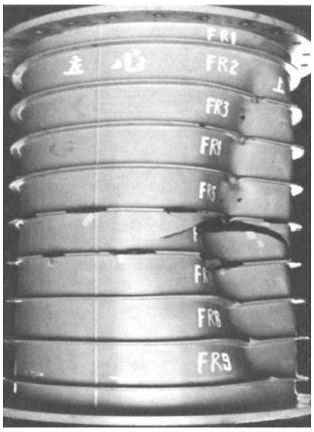	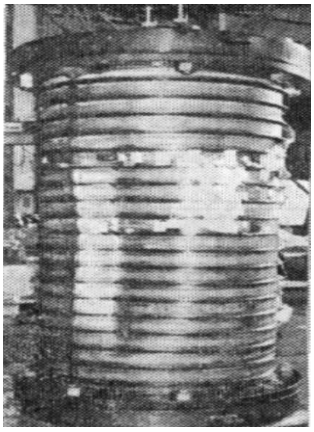	7 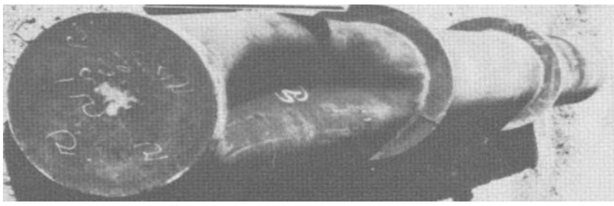 8 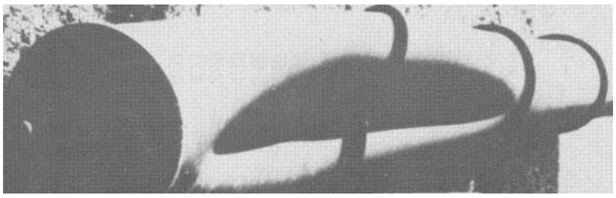	

stiffener and the close spacing between them. It appears that model no.1 is designed to acquire those yielding where the stiffener parameter h_w/t_w is relatively small, and the spacing is narrow ($L_s/L_c = 0.09$) compared to its overall length. The local buckling may occur on the moderate length of the cylinder to its radius with a wider space of stiffener, while also having a relatively thin shell thickness. Consequently, interframe buckling or local buckling occurred in model no. 2, 4, 7. The overall buckling shown in model no. 5, 6, 8 are categorised as the relatively long cylinder with a narrow stiffener space, and moderate or thick shell thickness. Finally, the failure mode interaction occurred where the local and overall buckling occurred after the collapse (model no.3).

The basic parameters from the benchmark of the test models are presented in Table 3. Among those models, the values of the highest and the lowest P_c were the results of models 7 and 2, respectively. This might be primarily attributed to the shell thin ratio (R/t), where model 7 exhibits the smallest ratio, implying that the shell is relatively thick compared to shell radius. These other parameters are treated as raw information to provide the adequate prediction on how the cylinder will fail.

3.1 Formulation of failure modes

The basic problem on thin-walled cylindrical shell under external pressures starts from two stresses that exist on the shell. They are the axial and circumferential stress, where the axial stress is half of the circumferential ones.

In reality, the collapse pressure typically exceeds the yield point of the material. It is necessary to obtain the approximation of the yield pressure according to the von Mises yield criterion, as stated by Eq. (1),

$$P_Y = \frac{\sigma_Y t}{R} \frac{1}{\sqrt{\frac{1}{4} - \frac{(1-\gamma G)}{2} + (1-\gamma G)^2}} \tag{1}$$

where the detail of the failure equation in this section is presented in the previous work (Cho *et al*. 2018b). In the local buckling mode, the failure was demonstrated by the loss of stability of the shell with several numbers of lobes occurring between the frames in the local area. The local buckling equation is a function from the von Mises solution

Table 3 Basic parameter of the benchmark test model

Base model	Basic parameters						Exp. Collapse pressure (MPa)
	L_c/R	R/t	h_w/t_w	L_s/t	L_s/L_c	$E/\sigma_Y.10^3$	P_c
1	2.02	61.00	3.70	11.66	0.09	0.63	8.96
2	3.46	114.38	6.41	41.67	0.11	0.76	1.84
3	2.65	100.00	8.97	50.00	0.19	0.67	2.16
4	3.35	99.12	4.08	53.12	0.16	0.60	2.69
5	3.00	65.33	4.63	21.73	0.11	0.37	6.23
6	3.86	99.50	4.80	20.00	0.05	0.37	4.50
7	24.70	17.93	7.04	139.64	0.32	0.75	9.32
8	24.45	30.00	5.30	184.93	0.25	0.74	2.77

to estimate the critical pressure of the radially loaded from the simply supported cylindrical shell presented as Eq. (2).

$$P_m = \frac{Et}{R}\left\{n^2 - 1 + \frac{1}{2}\left(\frac{\pi R}{L_s}\right)^2\right\}^{-1} \left[\left\{n^2\left(\frac{L_s}{\pi R}\right)^2 + 1\right\}^{-2} + \frac{t^2}{12R^2(1-v^2)}\left\{n^2 - 1 + \left(\frac{\pi R}{L_s}\right)^2\right\}^2\right] \tag{2}$$

The overall buckling failure mode consists of the shell and frame deformation in one compartment length. It occurs when the stiffener is relatively small compared to the shell thickness and the cylinder is relatively long. It is characterised by long wavelengths in both the circumferential (n) and axial directions. Bryant's two-term approximation to the overall buckling pressure is given in Eq. (3).

$$P_n = \frac{(n^2-1)EI_c}{R^3 L_s} + \frac{\left(\frac{Et}{R}\right)}{\left[n^2 - 1 + \frac{1}{2}\left(\frac{\pi R}{L_c}\right)^2\right]} \left\{\frac{1}{\left[n^2\left(\frac{L_c}{\pi R}\right)^2 + 1\right]^2}\right\} \tag{3}$$

The last mode that should be considered is the stiffener tripping. This mode is marked by the rotation a stiffener away from perpendicular with the shell. Design rules such as PD 5500 address this failure as a separate criterion that has to conform to the procedure to satisfy the overall buckling as Eq. (4).

$$P_t = \frac{\sigma_t P_{yf} R_s}{\sigma_y R_f} \tag{4}$$

$$\left(\frac{P_C}{\rho_L P_m} + \frac{P_C}{\rho_{OA} P_n} + \frac{P_C}{\rho_T P_t}\right)^2 + \left(\frac{P_C}{P_Y}\right)^2 = 1 \tag{5}$$

Next, the new formulation to estimate the ultimate strength is given by Eq. (5). It is the failure mode interaction form where all of the failure terms were included. Those terms provided the quadratic linearity of the local buckling pressure (P_m), overall buckling pressure (P_m), tripping pressure (P_t), and yield pressure (P_Y). The thickness variation, initial shape, and material imperfection, as well as the residual stress due to welding, were assumed to be evaluated by the knockdown factor, given as the knockdown factor for local buckling (ρ_L), overall buckling (ρ_{OA}), and tripping (ρ_T) in Eqs. (6–8).

$\rho_T = 2.7374\ Exp\ \{0.0088\ (L_s/R)(\sqrt{(L_s/t)}\}$, *for tripping* (6)

$\rho_{OA} = 1.055\ Exp\ \{0.167\ (h_w/t_w)(E/1000\sigma_Y)\}$, *for overall buckling* (7)

$\rho_L = 0.674\ Exp\ \{0.0006\ (h_w/t_w)(\sqrt{R\ L_S}/t)(E/1000\sigma_Y)\}$, *for local buckling* (8)

4. Finite element modelling and benchmarking

The benchmark for the ultimate strength test from the test model was developed within the framework of the nonlinear finite element routines, ABAQUS. This analyses were focused on how the nonlinear factors which effect on the structural buckling. As it is recommended in the ref. (Aghajari *et al.* 2011; ISSC 2015; Bai *et al.* 2017), those factor such are the change of geometric shape and material nonlinearity due to shell forming and stiffener welding effect have to be implemented in the ultimate strength analyses. After it has been verified with the test results, this FEA methodology will be used to further validate the failure mode criterion where the various geometric parameters are assessed from the base-tested model.

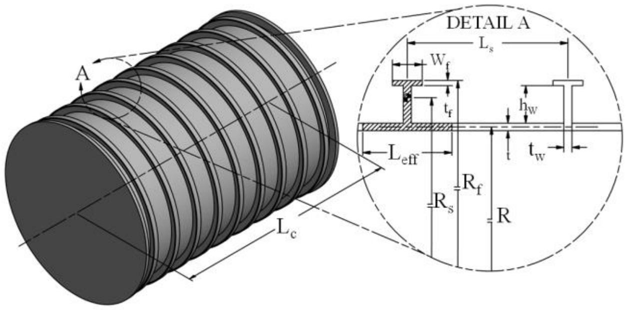

Fig. 2 Basic geometrical notation for the basic failure mode formulations

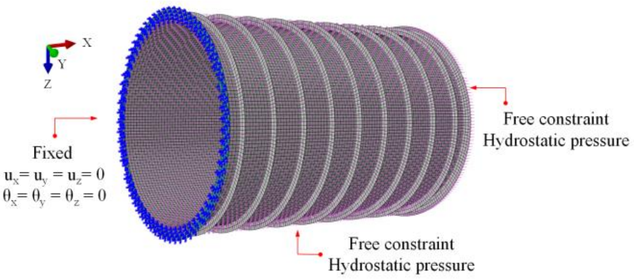

Fig. 3 Finite element mesh, load and boundaries for ultimate strength analyses

The model was discretised with the shell element (S4R) with reduced integration and hourglass control. Before performing the benchmark analyses much further, mesh convergence studies were performed with the result of the ratio of the global mesh size to the shell thickness of 2.0. Fig. 3 shows the detail of the typical finite element model that is used in the benchmark analyses. The boundary conditions follow the tested model in the actual condition where one side of the cylinder is fixed to the end flange and bolted to the chamber, while the other end is in the free condition. The material in the benchmark analyses was assumed to be elastic-perfectly plastic with Young's modulus and yield stress, as shown in previous section. To analyse the collapsed pressure, the static solver of the Riks arc length method is utilised.

4.1 Cylindrical shell forming

In the first step of the analysis, the nodes at one edge of the cylinder are tied to the reference node in the mid-edge to which a rotation is applied. At the other edges, all degrees of freedom of the nodes are restrained. In the second step, the rotation is removed and the plate springs back elastically. Iteratively, the required overbend curvature was determined. These two steps were performed in a quasi-static analysis that included large deformations and plasticity. In Fig. 4, the flat plate before and after cold bending is shown.

When a plate is rolled to a radius R, the residual stress distribution can easily be calculated if the material is assumed to be ideal elastic-plastic and Bausinger effects are ignored. It has a zig-zag distribution through its thickness with compression σ_1 at $0.65t$ between the concave surface and the mid-thickness. For instance, Fig. 5 shows the stress distribution path through the thickness from the particular quarter shell for base model 4 for σ_Y = 345 N/mm^2 and E = 206000 N/mm^2. Those average stresses were obtained from the simulation. The parameter of maximum stress due to cold-rolling is $\sigma_1/\sigma_Y = 0.63$. Therefore, in hoop compression, the maximum stress would start to exceed the yield stress at an applied pressure or average stress only 37% of that to cause a general yield in an initially stress-free cylinder.

4.2 Welding effects of the ring-stiffener

In the ultimate strength problem, the welding treatment has a significant effect that is associated with the

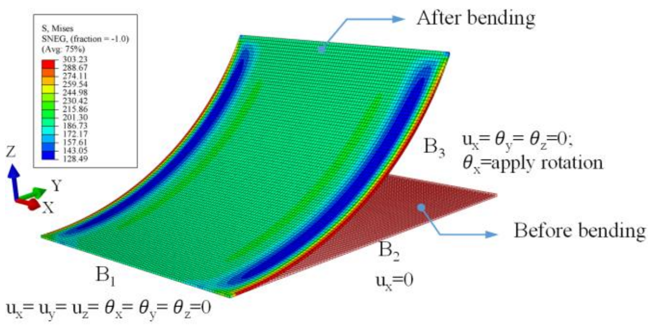

Fig. 4 Residual circumferential stress exhibited on the flat plate section after cold bending

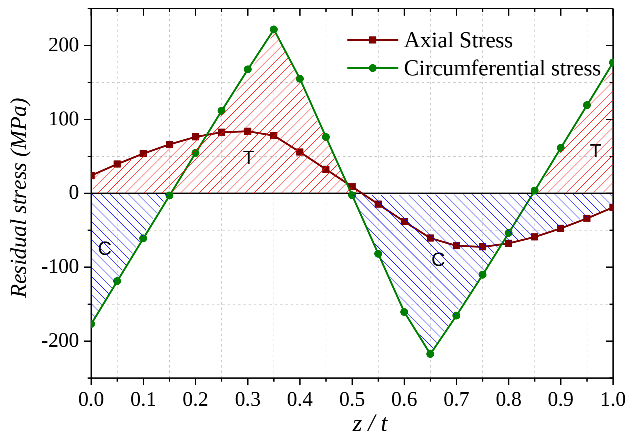

Fig. 5 Residual stresses distribution through shell thickness obtained from the simulation

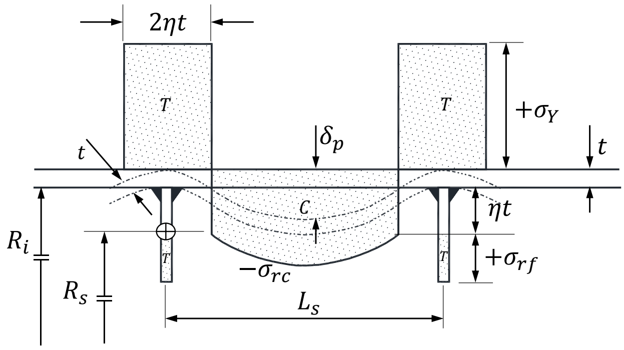

Fig. 6 Residual stress estimation on the internal flat bar ring-stiffened cylinders

distortion and residual stresses. The local distortions will be accumulated as the sinusoidal strength variation between the stiffeners. The reduction effects on the ring-stiffened cylinder shall be carefully considered from the design view point as written in Eqs. (9–12). The hungry-horse pattern of the welding shrinkage is described in Fig. 6. The important imperfections were σ_{rc}, σ_{rf}, δ_p, defined as the maximum or mid-region residual compressive stress, residual tension stress in ring-frame, and interframe shell distortion, respectively. The other substantial parameters that are experienced in submarine structures and some offshore jacket structures as is recommended for the 'wrap-up' welding distortion is 10% relative to the shell thickness

($\delta_p/t \cong 0.1$), and the welding tension block width parameter is equal to 4 (η=4).

$$\sigma_{rc} = \sigma_{rc1} + \sigma_{rc2} \tag{9}$$

$$\sigma_{rf} = \frac{\dfrac{2\delta_p E}{\pi R}}{\left[1 + A_f \left(\dfrac{R}{R_c}\right)^2 / (L_s t)\right]} \tag{10}$$

$$\sigma_{rc1} = 2\eta\sigma_Y t / (L_s - 2\eta t) \tag{11}$$

$$\sigma_{rc2} = \sigma_{rf} - \delta_p E / R \tag{12}$$

where R_i is the inner radius and the other parameters are similarly described in the previous section.

To measure the effect of the welding residual stresses, the constant stress distribution from the equation above is included in the finite element analyses as the initial stress. The corresponding elements were first modelled as the yield tension areas where the width is described in the $2\eta t$-covered area of the weld, and the remaining element between the stiffeners applies for the residual compressive stress σ_{rc} as well as the residual tension stress in the ring stiffener σ_{rf}. Subsequently, the calculated stress are given at the corresponding element.

Fig. 7 shows the average circumferential stress $\sigma_\emptyset$ distribution at the yield tension element produced by the simulation. It indicates that the stress near the welding zone a width $2\eta t$ rises as much as the yield strength σ_Y of the material. It is not surprising that the welding temperature that is approximately twelve times greater than the range caused the yield in the resisted thermal expansion of the steel. This tension block causes curve-down as much as δ_p for the internal welded stiffener as Fig. 8 (a), and curve-up for the external welded stiffener Fig. 8 (b).

4.3 Initial shape imperfection

Most pressure hulls are typically considered the maximum radial shell imperfection, which equals to 0.005 times the radius of the shell (Cerik 2015). The initial shape imperfection is an inevitable spot along the shell due to the welding fabrication processes of the ring stiffener to the shell. It occurs in any real of pressure vessels as all of those structures were fabricated instead of perfectly machined. One of the reliable solutions for modelling the imperfection was based on spline curving and fitting techniques of the measured cylinder node (Cho *et al.* 2018a), and the other approach was based on the decomposition of the measured radii using the Fourier expansion (Kendrick 1977). However, on quite large structures, these methods appear impractical. Therefore, in this benchmark analysis, the imperfection in the geometry is generated by the controlled magnitude using the eigenmode analysis.

Fig. 9 shows the imperfection sensitivity results of the idealised short, intermediate, and the long ring-stiffened cylinder from the corresponding tested models. The single imperfection is the assumed eigenmode imperfection that manifests only from the first mode. The combined imperfection referred to the inclusion of another significant mode of shape imperfection. It was found that the combined imperfection of the local and overall modes reduced the

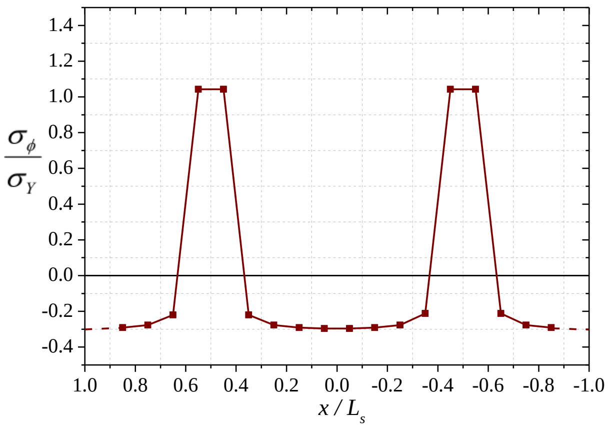

Fig. 7 Welding residual stresses distribution obtained from analyses of base model no. 3

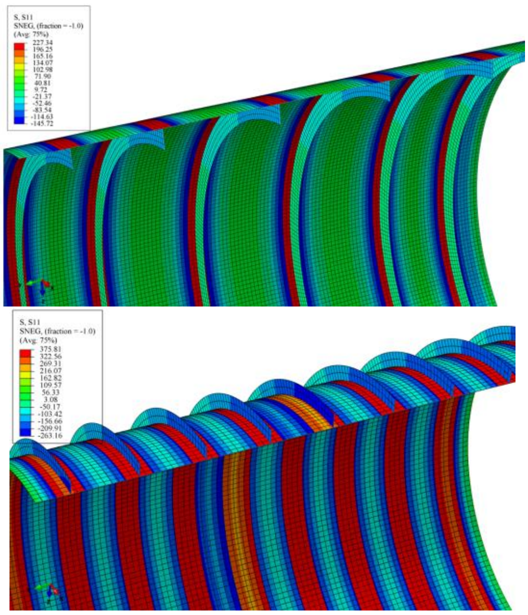

Fig. 8 Welding shrinkage action in the numerical analyses: (top) base model no. 3, and (bottom) base model no. 5

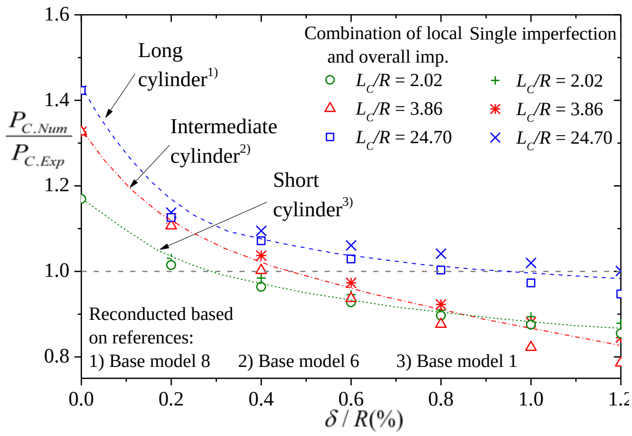

Fig. 9 Imperfection sensitivity for short, intermediate and long test models

Table 4 Comparison of deformed shape using single and combine imperfection for intermediate length model

a) Single imperfection	b) Combine imperfection	Base model no.6
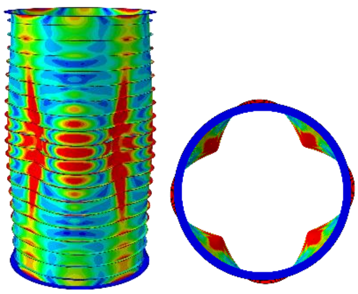	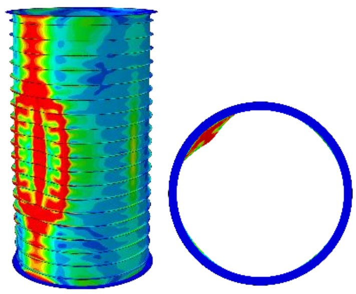	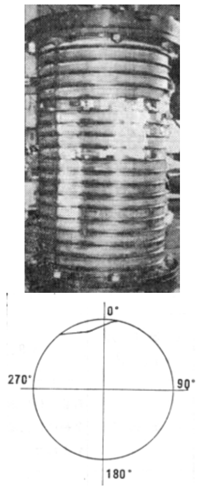
n = 4	n = 1	n = 1
m = 1	m = 1	m = 1

predicted collapse pressure. The effect of reduction become large as its magnitude increased. For the long model case, the level of magnitude in the tested model relied on more than 0.5% (noted 0.8%) of the shell radius, whereas the short model showed less than that value (0.3%R). In between those were the typical magnitudes for the intermediate length of the ring-stiffened cylinder.

It also found that the combined imperfection reduces the dominant shape of the single imperfection where the actual deformed shape would be achieved. As described in Table 4, the single imperfection of the intermediate model is dominant by the overall shape imperfection. When the first local mode imperfection is introduced in the combined imperfection, the actual shape can be obtained and the final shape is reached at $n=1$ and $m=1$. Here, n, m are the full waves at the circumferential and half waves at the longitudinal direction of the cylinders, respectively.

4.4 Benchmark analyses

To verify the FE analyses procedures above, eight benchmark analyses of ring-stiffened cylinder ultimate strength test were performed. For verification, the pressure against the strain obtained from the test and the FEA results are compared. Fig. 10 and 11 show the detailed comparison of the base model no. 3, and base model no. 5, respectively. They describe the local strain measurement, comparison of the pressure versus strain values, and deformed shape obtained from the test results and FEA. Overall, the FE analyses succeeded in predicting the nonlinear behaviour of the test models.

The test result for the base model 3 (RS-I) shows the interactive failure mode where the overall failure along the cylinder length occurred with partial lobes between the frame at several areas. The numerical models succeeded in predicting the occurrences of overall failures but the local buckling lobes were not as exact as the test models. For instance, the local axial strain between the test and numerical shows a small differences about 20 %. The most probably reason is due to the rigidity of the end plate from the actual cylinder which could affect the axial compression on the structure. The perfect uniform thickness which use in the numerical modelling also play a role in the axial compression response. Another reason can be strongly attributed to errors in the actual initial shape imperfection and the variation in the shell thickness along the cylinder, where the idealised assumption (eigenmode imperfection and initial welding stress) were not sufficient to determine the interactive buckling failure shape.

In the case of base model 5(W3), the overall failure is dominant as the post-collapse shape. The nonlinear responses were concentrated in the mid-bay of the cylinder. It grows as the pressure increases, leaving a permanent damage where the shell and ring stiffener failed as a unit. The compute strain values in Fig. 11(b) indicate that the FE model was successful at predicting the behaviour. The circumferential strains are the greatest at the outer shell rather than at the inner shell. This indicates the largest compressive stress arising from the bending moment induced by the overall imperfection. The predicted collapse pressure was within 4% of the experimental collapse pressure.

The results from the predicted values using the design equations of the others benchmark test models, are provided in Table 5. All of the FEA results have smaller collapse pressure than the test. The reduction resulted from the combination of initial shape imperfection and welding residual stress that applied in the numerical analyses may contributed to the ultimate strength prediction. However, the accuracies for the entire set of nonlinear FEA and the ultimate strength formula shows good results, with errors of 4.32 %, and 9.56 %, respectively.

5. Failure mode verification studies

The results of the numerical analyses in the previous section confirmed that the nonlinear computation can forecast the failure mode of the structure as the actual ones. Further numerical studies were performed on the chosen actual base model case. The four basic parameters selected are the shell thickness, stiffener height, stiffener spacing, and overall length of the cylinder. It will subsequently be used parametrically to prove the effectiveness of the failure mode criterion. Further numerical results will support that more realistically by only subtracting the fluctuation of the parameter values. The failure mode would subsequently be changed.

To demonstrate the development of the failure mode by its criterion, a parametric series using 240 cases of basic parameter variations was performed using Eq. (5), and a few chosen cases were verified through nonlinear FEA where the procedure were established earlier. The parameter case studies are presented in Table 6. The value presented in those tables were non-dimensionalised to its original value.

5.1 Effect of overall length variation

The first verification is performed when the overall length L_c of cylinder is decreasing. In Fig. 12, six base models were modelled and calculated using the criterion P_c/P_Y against P_n/P_m. There is a clear marking using red line that indicates the failure zone. For the overall buckling, the left side red line marking for the value P_n/P_m is less than 1.0. The right side mark borders the local buckling for P_n/P_m larger than 2.5. The transition zone that is for shell yielding failure and interaction mode between the local and overall failure indicated the remaining zone in between 1.0 to 2.5. Hence, the ultimate strength and P_n/P_m of the base model will show the dominant failure mode. For instance, the base model no. 5 and 6 failed in the overall failure mode marked by the P_n/P_m equal to 0.82 and 0.34, respectively. Further, the base models no.2 and 4 collapsed in the form of local failure, as shown by the P_n/P_m values of 2.92 and 4.00, respectively.

The criteria above demonstrates the development of the failure mode. It shows how the failure mode of the structure could change when the model becomes shorter. As shown, a shorter cylinder will tend to fail in the local buckling failure. In addition, numerical analyses were used to verify this finding. Fig. 13 shows the numerical analyses results of base model no.5 using various overall length. The corresponding post-collapse shapes are marked with numbered bullets of six length variations in the range of L_c/R of 3.00 decreased to 0.40. Image ① corresponds to actual model no.5, where it is clear that the failure mode is the same as the test results (Table 2). It matches well with the associated criteria ($P_n/P_m < 1.0$). As the overall length decreased, its modes moved from the overall to local. It also strengthens the collapse capacity. In image ② to ④ at L_c/R = 2.20 to 1.25 the overall failure is still dominant until it involves the minimum four frames with the similar stiffener spacing as the origin. As it decreased more, the interactive mode is shown in image ⑤ where the three ring-stiffened shells lost their local stability and spread over the total compartment. In this case, the P_n/P_m criterion is 2.30. As stated, this is in the failure mode interaction region. Finally, in image ⑥, local failure is exhibited in this model as its value shows the largest P_n/P_m of 3.18. It is beyond the red line border indicating the local failure region.

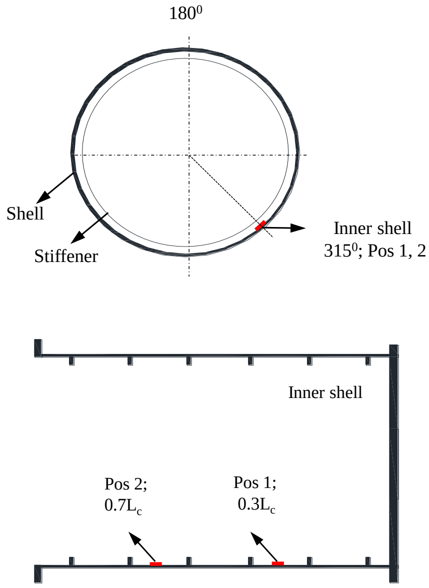

(a)

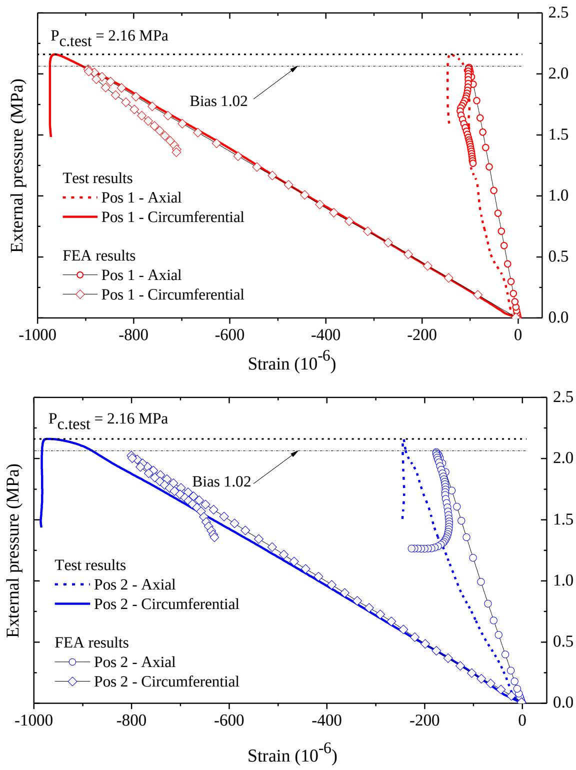

(b)

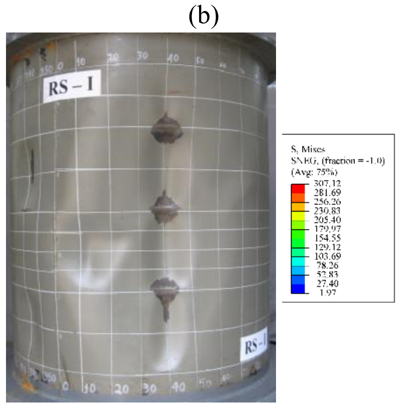

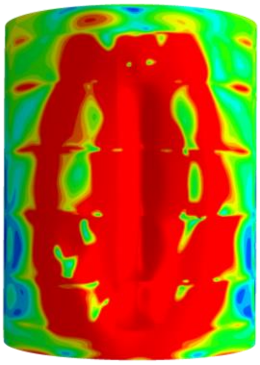

(c)

Fig. 10 Validation of numerical results through pressure and strain response for the base model no.3: (a) Strain position, (b) Deformed shape comparison, (c) Pressure – Strain curve validation

Table 5 Benchmark results of the numerical and analytical method

Collapse pressure $-P_c$ (MPa)		Base model 1	2	3	4	5	6	7	8	Mean	Accuracy (%)
Test		8.96	1.84	2.16	2.69	6.23	4.50	9.32	2.77	-	-
FEA		8.06	1.76	2.12	2.51	5.98	3.97	9.07	2.76	-	-
New formula Eq. (5)		7.91	2.05	2.09	2.81	6.51	3.93	8.76	3.06	-	-
X_m	FEA	1.11	1.04	1.02	1.07	1.04	1.13	1.03	1.00	1.06	95.68
	New formula	1.13	0.90	1.03	0.96	0.96	1.14	1.06	0.91	1.01	90.44

$X_m = P_c$ test / P_c prediction

Table 6 Parameter case studies from actual base model as submarine pressure hull representative

Base model	Case studies data range (respect to original value): Overall length (Fig. 12-13)	Shell thickness (Fig. 14-15)	Stiffener height (Fig. 16-17)	Frame spacing (Fig. 18-19)
1	2.00 - 0.32L_c	1.96 - 0.68t	0.50 – 1.50h_w	0.28 – 1.84L_s
2	5.26 - 0.67L_c	2.50 - 0.83t	0.48 – 1.20h_w	0.20 – 2.90L_s
3	4.72 - 0.60L_c	1.75 - 0.75t	0.50 – 1.32h_w	0.20 – 4.50L_s
4	3.54 - 0.75L_c	1.16 - 0.51t	0.20 – 0.66h_w	0.11 – 1.00L_s
5	1.09 - 0.14L_c	2.00 - 0.45t	1.00 – 2.30h_w	0.61 – 6.75L_s
6	0.52 - 0.08L_c	1.20 - 0.30t	1.00 – 3.83h_w	20 – 4.00L_s

5.2 Effect of shell thickness variation

Fig. 14 shows effect of shell thickness variation on the failure modes. For instance, base model 6 shown by notation L_c/R 3.86 varied the shell thickness from 1.20t decreased to 0.30 t from the original shell thickness 5 mm. The corresponding range for the others base model were written in Table 6. Here, the shell thickness started from the thick ones where the overall buckling is likely to occur, and as the shell thickness becomes relatively thin, the local buckling will be dominant. The associated criteria were remarked by the vertical red line under the condition of P_n/P_m value. The black bullet circles show where the actual base model was laid on. From this figure, the failure modes of the base model was in good agreement with the test results.

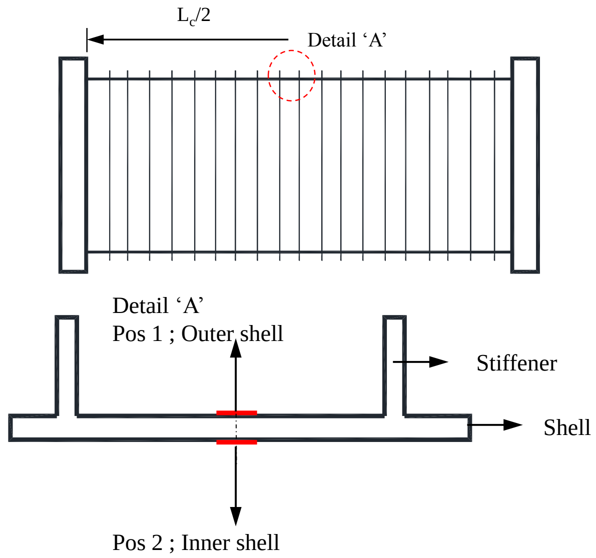

(a)

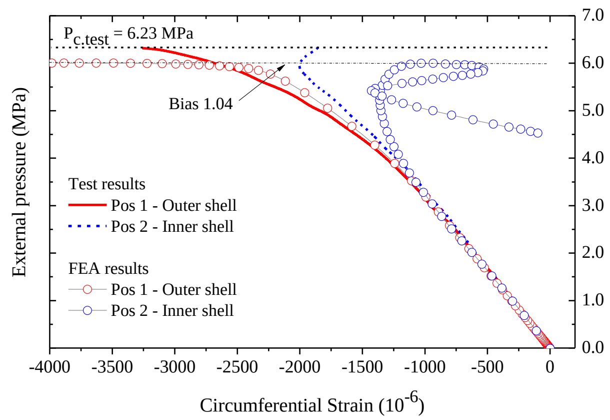

(b)

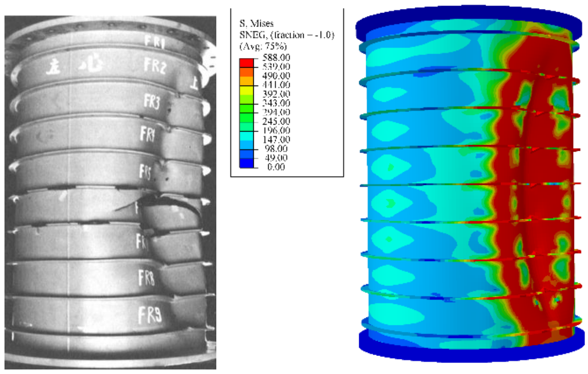

(c)

Fig. 11 Validation of numerical results through pressure and strain response for the base model no. 5: (a) Strain position, (b) Deformed shape comparison, (c) Pressure – Strain curve validation

The validation of these case studies was performed through numerical analyses. Fig. 15 shows the post-collapse images from base model no. 6 under decreasing shell thickness. Six cases were noted from R/t ratio of 100, 190, 220, 250, 270, and 300. It starts from the actual base model no.6 in image ① with R/t ratio equal to 100. In this case, the overall failure is dominant where agrees well with the actual test results. The associated criterion of P_n/P_m= 0.34 is in the overall failure region. As the shell thickness decreases from an R/t ratio of 190 to 220, the overall failure is still dominant as shown in image ② and ③. It has subsequently decreased approximately 0.4t in image ④ for an R/t ratio of 250, and the overall failure domination were reduced by the local buckling spreading between the frames. In this case the P_n/P_m is shown in the region of the interactive zone. As shown in image ⑤ and ⑥, the thickness continued to decreased for R/t of 270, 300 with the thickness 0.36t and 0.30t, respectively. The local buckling has retaining and several other lobes between the frames.

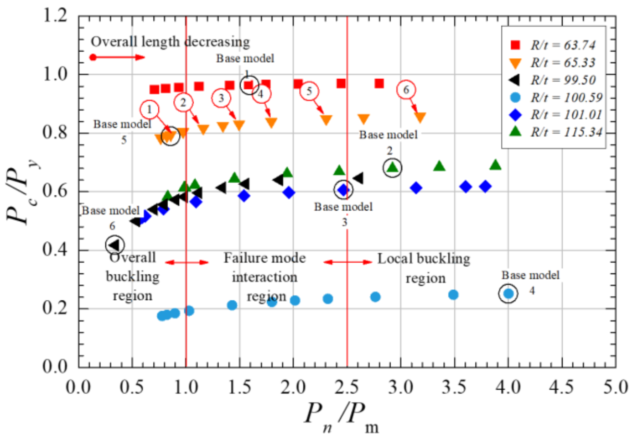

Fig. 12 Evaluation of the failure modes criteria under decrease in overall length

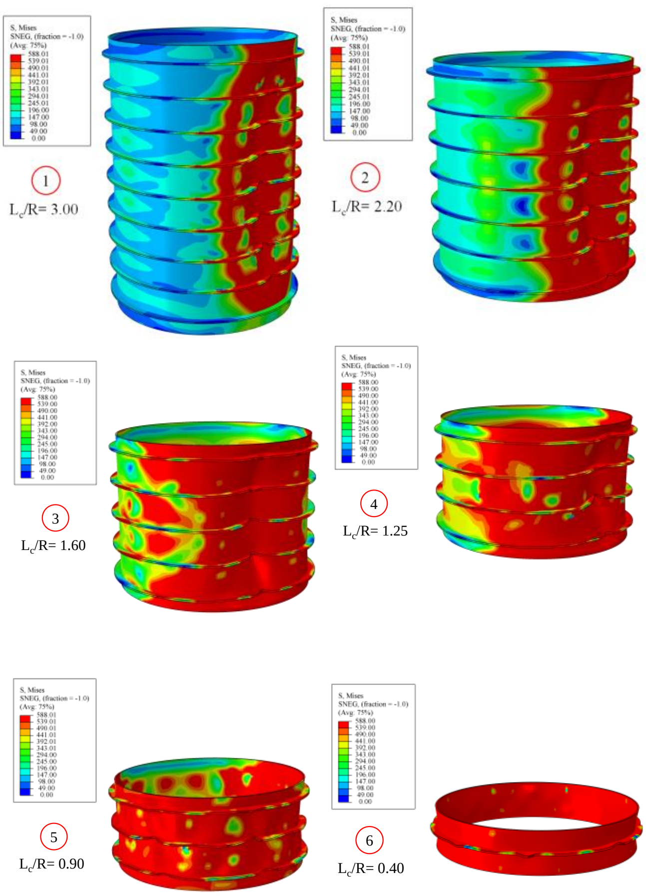

Fig. 13 Failure modes response from base model no. 5 owing to overall length variation

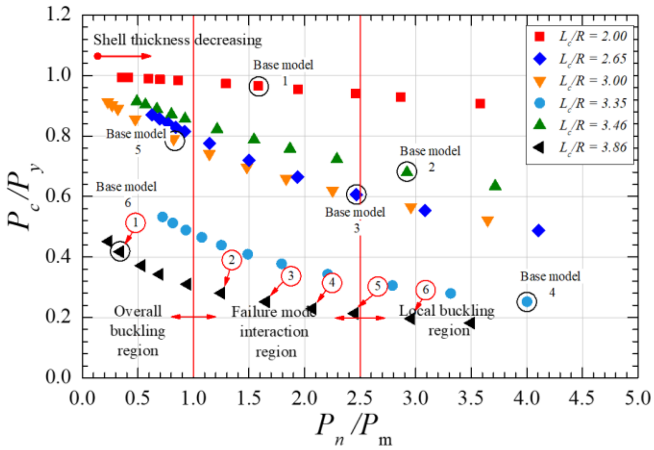

Fig. 14 Evaluation of the failure modes criteria under decrease in shell thickness

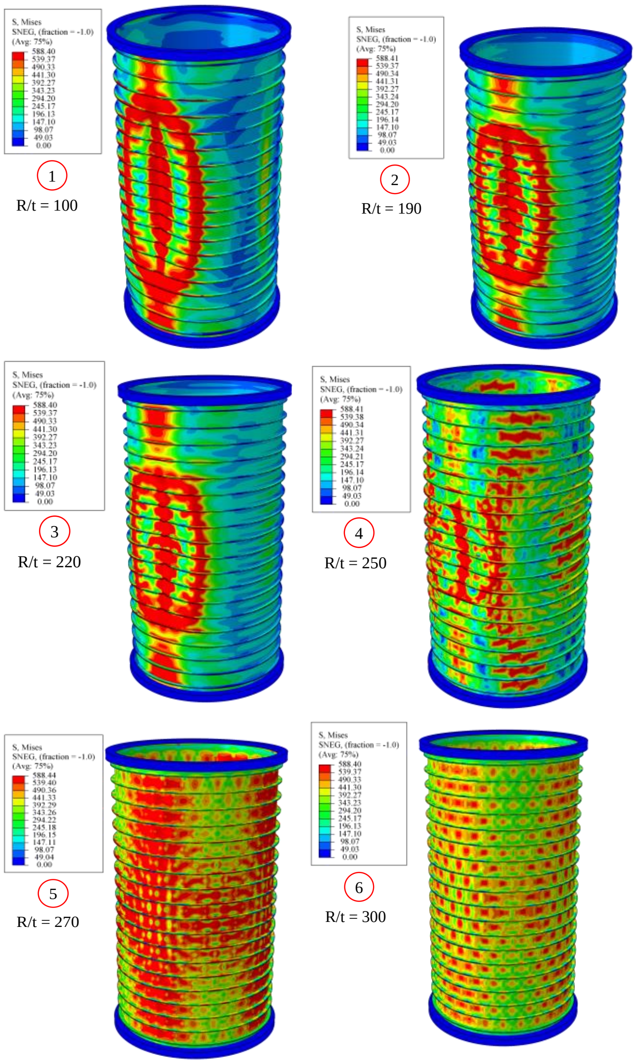

Fig. 15 Failure modes response from base model no. 6 owing to shell thickness variation

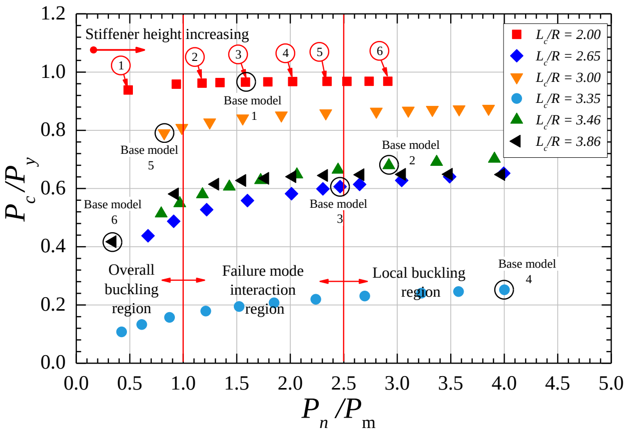

Fig. 16 Evaluation of the failure modes criteria under increase in stiffener height

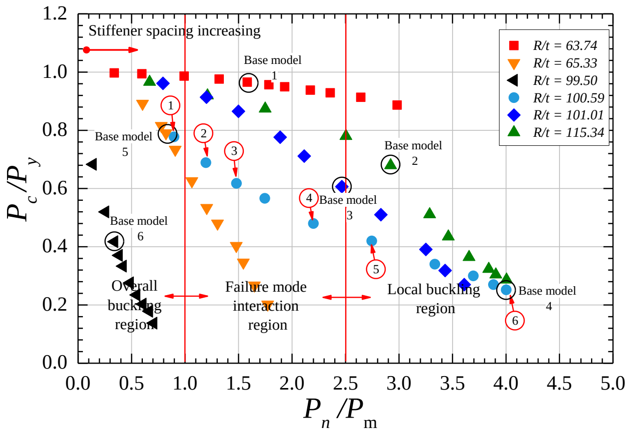

Fig. 18 Evaluation of the failure modes criteria under increase in stiffener spacing

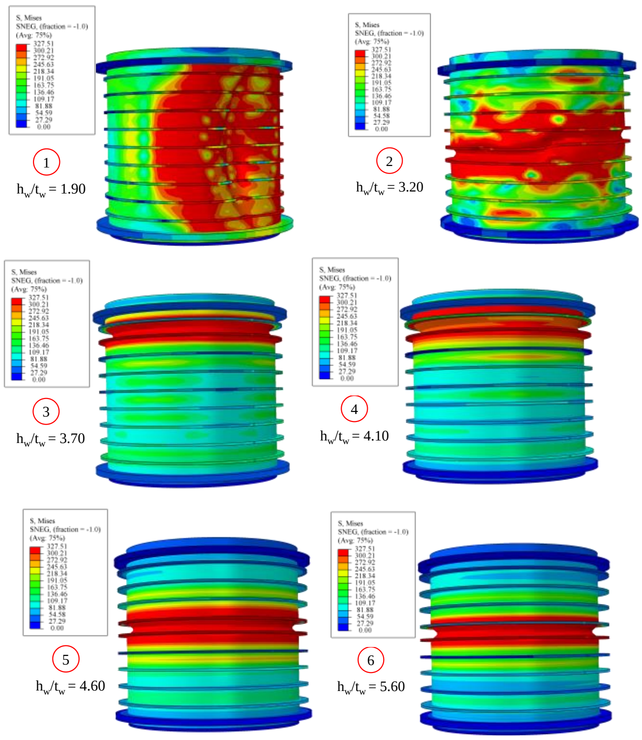

Fig. 17 Failure modes response from base model no.1 owing to stiffener height variation

5.3 Effect of stiffener height variation

Fig. 16 shows the effect of increasing the stiffener height on the failure mode. The base model was the same as the previous one. From this figure, we found that by increasing the stiffener height until a certain size, the collapse pressure showed no significant effect. For instance, in base model no. 5, the variation was made from 1.00 to 2.30 times the original height. As the height is increased from the original value to 1.50 h_w the collapse pressure gradually increased. Subsequently, for 1.60 to 2.3 times the original height, the collapse pressure remained the same. It is assumed that when a ring- stiffener becomes unstable, it cannot provide adequate support for the shell. However, further study is required to confirm this hypothesis.

Fig. 17 illustrates the stiffener height variation for base model no. 1. The first variation in image ① shows h_w/t_w ratio 1.90 with the P_n/P_m equal to 0.49. Therefore, the overall failure is dominant. The next images show the increasing stiffener height at h_w/t_w reaching 3.20 in image ②, and the failure mode is changed. The mode of interaction between the overall failure and yielding is shown. Subsequently, after increasing h_w/t_w to 3.70 in image ③ the shell yielding failure is dominant. This is denoted as the test results of the base model 1. It is subsequently continued by images ④ to⑤ that varied the value of the stiffener height for 1.10, 1.25, and 1.50 times of the original height. However, for the last three cases, the numerical results show that the shell yield failure is still dominant even when the criteria show that for the last case, the value of P_n/P_m was that of the local buckling region. This is because the early assumption for a longer stiffener would have no significant effect on maintaining the circularity of the shell. It was subsequently similar for the failure modes.

5.4 Effect of stiffener spacing variation

The stiffener spacing might affect the flexural rigidity of the combined cylinder and stiffener. Therefore, if the rings are sufficiently stiff to maintain the roundness during the loading, the shell may be considered as divided into a series of short shells whose length is the distance between the rings. To clarify this assumption, the spacing will be varied among the base models. The models are similar as those of the previous case. Fig. 18 demonstrates the case of increasing the stiffener spacing that not only gave the reduction in collapse pressure but also affected the failure mode evolution.

As highlighted in the figure for base model no. 4, the variation starts from 0.11 to 1.00L_s. The criteria result is that for a narrow spacing, the shell yielding failure is dominant. Even in this case, the criteria falling in the regime of overall buckling but due to the original stiffener is relatively sturdy and strong, and the shell yield is dominant. In contrast, a wider spacing will cause local failures and this agrees well with the criteria. For the actual case, base model no.4 is failed by the local buckling.

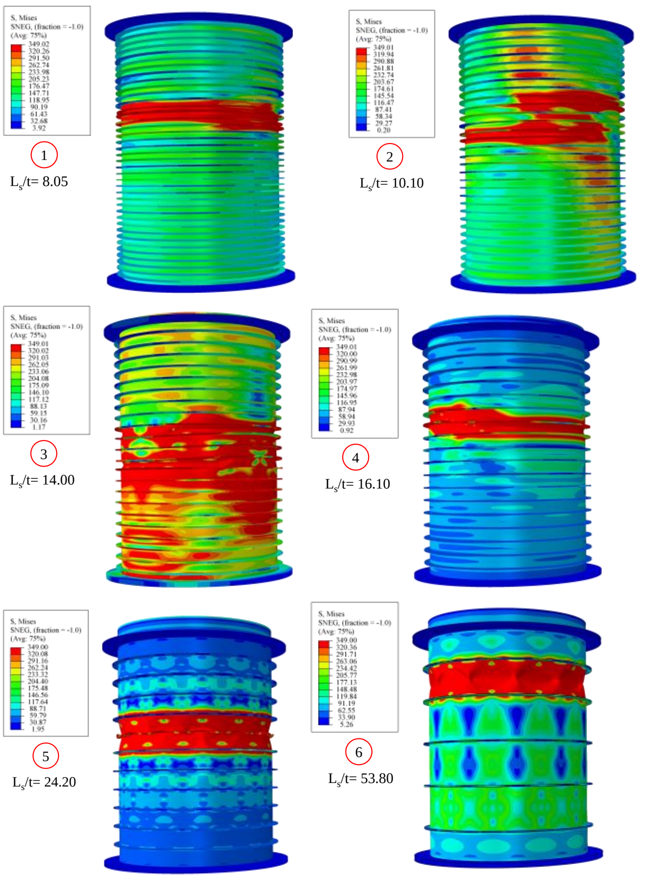

Fig. 19 Failure modes response from base model no. 4 owing to stiffener spacing

Fig. 19 shows the post-collapse images obtained from the simulation from base model no. 4 for various stiffener spacing. In image ① the spacing was only 11% of the original size (180.6 mm), causing the failure mode to change from local buckling to shell yielding. In image ② to ④, the failure mode interactive is dominant. In this case, the spacing was varied from 0.13, 0.16, 0.19L_s with respect to the original size. It shows good agreement with the criteria where those three cases were in the interactive mode region ($1.0 < P_n/P_m < 2.5$). As shown in images ⑤ and ⑥, the local failure occurred as the associated criteria were larger than 2.50, especially for the test results of model 4 where the failure is represented well in image ⑥.

6. Concluding remarks

It is shown that basic parameters such as shell thickness, stiffener height, stiffener spacing, and overall length of the cylinder would govern the failure mode of the structure. It is clearly clarified through the normalised characteristic pressure such as P_n/P_m that can be used as the criterion to predict the failure modes, such as local buckling, overall buckling, shell yielding, and failure mode interaction between local and overall buckling. The overall buckling will occur if the ratio of P_n/P_m is less than 1.0. The local buckling will be dominant if the criterion shows a value higher than 2.5, whereas in the region of 1.0–2.5, the failure mode interaction will occur.

The present criteria would render the engineering design level of ring-stiffened cylinders complete in terms of practical purposes, especially when the designer was involved in such rules and guidelines from other classifications related with the scantling requirements for submarine pressure hull, where the failure mode of the structure was not clearly predicted. However, to provide better understanding, the trade-off study among the basic parameters of ring-stiffened cylinder would yield better assessments and optimised designs.

The ultimate strength assessment from the proposed formulae and the nonlinear FEA was demonstrated against the test results from the literatures. It can be concluded that if the geometric and material parameters are well defined, the accuracies of the available method can be improved. Although some conservatism exist in the proposed ultimate strength formula, it has implicitly considered the reduction factor that significantly affect the ultimate strength such as the welding residual stresses and initial imperfection. Therefore, in the early design stage, the ultimate strength formula and its criteria can be a design tool. In nonlinear FEA, careful attention must be given to the magnitude level of the assumed imperfections, which may be triggered on the over or underestimated prediction. As no update published experiment exists in the real case of the submarine pressure hull structures, the accurate level of the imperfection magnitude calibration as well as the welding residual stress would be difficult to achieved.

Acknowledgements

The first author would like to gratefully acknowledge the financial support from The Research and Innovation in Science and Technology Project (RISET-Pro) from Ministry of Research, Technology and Higher Education Republic of Indonesia [Loan number 8245-ID].

References

Aghajari, S., Showkati, H. and Abedi, K. (2011), "Experimental investigation on the buckling of thin cylindrical shells with two-stepwise variable thickness under external pressure", *Struct. Eng. Mech.*, **39**(6), 849-860. https://doi.org/10.12989/sem.2011.39.6.849.

Araar, M. and Julien, J.F. (1996), "Buckling of cylindrical shells under external pressure proposition of a new shape of self-stiffened shell", *Struct. Eng. Mech.* **4**(4), 451-460. https://doi.org/10.12989/sem.1996.4.4.451.

Bai, X., Xu, W., Ren, H. and Li, J. (2017), "Analysis of the influence of stiffness reduction on the load carrying capacity of ring-stiffened cylindrical shell", *Ocean Eng.*, **135**, 52-62. https://doi.org/10.1016/j.oceaneng.2017.02.034.

Bryant, A.R. (1954), "Hydrostatic pressure buckling of a ring-stiffened tube", NCRE Report No. 306; Naval Construction Research Establishment, United Kingdom.

B.S.I, PD 5500 (2003), Specification for Unfired Fusion Welded Pressure Vessels, British Standards Institution, London, United Kingdom.

Cerik, B.C. (2015), "Ultimate strength of locally damaged steel stiffened cylinders under axial compression", *Thin-Walled Struct.*, **95**, 138-151. https://doi.org/10.1016/j.tws.2015.07.004.

Cho, S.R., Muttaqie, T., Do, Q.T., Kim, S., Kim, S.M. and Han, D.H. (2018a), "Experimental investigations on the failure modes of ring-stiffened cylinders under external hydrostatic

pressure", *Int. J. Nav. Archit. Ocean Eng.*, **10**(6), 711-729. https://doi.org/10.1016/j.ijnaoe.2017.12.002.
Cho, S.R., Muttaqie, T., Do, Q.T., So, H.Y. and Sohn, J.M. (2018b), "Ultimate strength formulation considering failure mode interactions of ring-stiffened cylinders subjected to hydrostatic pressure", *Ocean Eng.*, **161**, 242-256. https://doi.org/10.1016/j.oceaneng.2018.04.083.
Fairbairn, W. (1858), "On the resistance of tubes to collapse", *Phiolosophical Trans. R. Soc.*, XXI. 389-413. https://doi.org/10.1098/rspl.1857.0056.
Frieze, P.A. (1994), "The experimental response of flat-bar stiffeners in cylinders under external pressure", *Mar. Struct.*, **7**, 213-230. https://doi.org/10.1016/0951-8339(94)90025-6.
Graham, D. (2007), "Predicting the collapse of externally pressurised ring-stiffened cylinders using finite element analysis", *Mar. Struct.*, **20**, 202-217. https://doi.org/10.1016/j.marstruc.2007.09.002.
ISSC (2015), "Committee III.1 ultimate strength", *Proc. 19th international Ship and oddshore Structure Congress,* Cascais, Portugal, September.
Kendrick, S.B. (1977), "Shape imperfections in cylinders and spheres: their importance in design and methods of measurement", *J. Strain Anal.*, **12**(2), 117-122. https://doi.org/10.1243%2F03093247V122117.
Kendrick, S.B. (1982), "Design for external pressure using general criteria", *J. Mechanical Science*, **24**(4), 209-218. https://doi.org/10.1016/0020-7403(82)90075-3.
Kirstein, A.F. and Slankard, R.C. (1956), "An experimental investigation of the shell-instability strength of a machined, ring-stiffened cylindrical shell under hydrostatic pressure (Model BR-4A)", *David Taylor Model Basin*, DTMB Report No. 997; Navy Department, Washington, D.C., U.S.A.
Lunchick, M.E. (1956), "Yield failure of stiffened cylinders under hydrostatic pressure", *David Taylor Model Basin*, DTMB Report No. 38; Navy Department, Washington, D.C., U.S.A.
Lunchick, M.E. and Overby, J.A. (1961), "Yield strength of machined ring-stiffened cylindrical shell under hydrostatic pressure", *Exp. Mech.*, 178-185. https://doi.org/10.1007/BF02323888.
MacKay, J.R., van Keulen, F. and Smith, M.J. (2011), "Quantifying the accuracy of numerical collapse predictions for the design of submarine pressure hulls", *Thin-Walled Struct.*, **49**, 145-156. https://doi.org/10.1016/j.tws.2010.08.015.
MacKay, J.R. and Van Keulen, F. (2013). "Partial safety factor approach to the design of submarine pressure hulls using nonlinear finite element analysis", *Finite Elem. Anal.,* **65**, 1-16. https://doi.org/10.1016/j.finel.2012.10.009.
Miller, C.D. and Kinra, R.K. (1981), "External pressure tests of ring-stiffened fabricated steel cylinders", *J. Pet. Technol.*, **33**, 2528-2538. https://doi.org/10.4043/4107-MS.
Morandi, A.C., Faulkner, D. and Das, P.K. (1996), "Frame tripping in ring stiffened externally pressurised cylinders", *Mar. Struct.*, **9**, 585-608. https://doi.org/10.1016/0951-8339(95)00020-8.
Morihana, H., Yamauchi, Y., Inoue, K., Nakamura, K., Takenaka, M. and Baba, K. (1990), "Research on general instability of cylindrical shells reinforced by ring-stiffeners under uniform pressure (2nd Report)", *J. Soc. Nav. Arch.*, **168**, 431-440. https://doi.org/10.2534/jjasnaoe1968.1990.168_431.
Ross, C.T.F., Gill-Carson, A. and Little, A.P.F. (2000), "The inelastic buckling of varying thickness circular cylinders under external hydrostatic pressure", *Struct. Eng. Mech.*, **9**(1), 51-68. http://doi.org/10.12989/sem.2000.9.1.051.
Ross, C.T.F. (1997), "Inelastic general instability of ring-stiffened circular cylinders and cones under uniform external pressure", *Struct. Eng. Mech.*, **5**(2), 193-207. http://dx.doi.org/10.12989/sem.1997.5.2.193.
Slankard, R.C. and Nash, W.A. (1953), "Test of the elastic stability of a ring-stiffened cylindrical shell, Model BR-5 (alpha=1.705) subjected to hydrostatic pressure", *David Taylor Model Basin*, DTMB Report No. 822; Navy Department, Washington, D.C., U.S.A.
Tokugawa, T. (1929), "Model experiments on the elastic stability of closed and cross-stiffened circular cylinders under uniform external pressure", *Proc. World Eng. Congr.*, **29**(651), 249-279.
von Mises (1929), "The critical external pressure of cylindrical tubes under uniform radial and axial load", *Stodolas Festschr*, 418-430.
Winderburg, D. and Trilling, C. (1934), "Collapse by Instability of thin cylindrical shells under external pressure", *Trans. ASME*, **11**, 819-825.
Yamamoto, Y., Homma, Y., Oshima, K., Mishiro, Y., Terada, H., Yoshikawa, T., Morihana, H., Yamauchi, Y. and Takenaka, M. (1989), "General instability of ring-stiffened cylindrical shells under external pressure", *Mar. Struct.*, **2**, 133-149. https://doi.org/10.1016/0951-8339(89)90009-9.
Yokota, K., Nanba, N., Yamauchi, Y., Urabe, Y. and Baba, K. (1985), "Research on general instability of cylindrical shells reinforced by ring stiffeners under uniform pressure (1st Report)", *J. Soc. Nav. Arch.*, **158**, 445-458.

CC